

# Response of the North Atlantic dynamic sea level and circulation to Greenland meltwater and climate change in an eddy-permitting ocean model

Oleg A. Saenko<sup>1</sup>  · Duo Yang<sup>1</sup> · Paul G. Myers<sup>2</sup>

Received: 26 July 2016 / Accepted: 7 December 2016 / Published online: 28 December 2016  
© The Author(s) 2016. This article is published with open access at Springerlink.com

**Abstract** The response of the North Atlantic dynamic sea surface height (SSH) and ocean circulation to Greenland Ice Sheet (GrIS) meltwater fluxes is investigated using a high-resolution model. The model is forced with either present-day-like or projected warmer climate conditions. In general, the impact of meltwater on the North Atlantic SSH and ocean circulation depends on the surface climate. In the two major regions of deep water formation, the Labrador Sea and the Nordic Seas, the basin-mean SSH increases with the increase of the GrIS meltwater flux. This SSH increase correlates with the decline of the Atlantic meridional overturning circulation (AMOC). However, while in the Labrador Sea the warming forcing and GrIS meltwater input lead to sea level rise, in the Nordic Seas these two forcings have an opposite influence on the convective mixing and basin-mean SSH (relative to the global mean). The warming leads to less sea-ice cover in the Nordic Seas, which favours stronger surface heat loss and deep mixing, lowering the SSH and generally increasing the transport of the East Greenland Current. In the Labrador Sea, the increased SSH and weaker deep convection are reflected in the decreased transport of the Labrador Current (LC), which closes the subpolar gyre in the west. Among the two major components of the LC transport, the thermohaline and bottom transports, the former is less sensitive to the GrIS meltwater fluxes under the warmer climate. The SSH difference across the LC, which is a component

of the bottom velocity, correlates with the long-term mean AMOC rate.

## 1 Introduction

The dynamic sea surface height (SSH), or sea level relative to geoid, reflects surface and, in many places, subsurface geostrophic circulation in the ocean (Wunsch 1997). A remarkable feature of the basin-scale SSH is the difference between the subpolar North Atlantic and the North Pacific (e.g., Levermann et al. 2005; henceforth L05). While in both these regions the SSH field is mostly negative (relative to the global mean), reflecting the predominantly cyclonic character of the large-scale ocean circulation, the mean SSH is considerably lower in the northern North Atlantic than in the North Pacific. This SSH difference between the two basins is thought to be maintained, at least in part, by the formation of deep water in the northern North Atlantic, associated with the Atlantic meridional overturning circulation (AMOC). Moreover, it has been proposed (L05) that there may exist a connection between the strength of the AMOC and SSH field such that a weaker AMOC is associated with a positive change in the basin-scale SSH in the northern North Atlantic. Scaling arguments (e.g., L05) do suggest a simple linear relationship between the AMOC rate and SSH change. To confirm their scaling, L05 ran a set of freshwater hosing experiments under present-day climate conditions, aimed at simulating a set of ocean states with progressively weaker AMOC. In their experiments the imposed freshwater fluxes were applied over a broad region of the northern North Atlantic, with values ranging from 0.05 to 0.4 Sv ( $1 \text{ Sv} = 10^6 \text{ m}^3 \text{ s}^{-1}$ ). L05 found, in particular, that in an extreme case of complete AMOC collapse, corresponding in their model to a freshwater flux of 0.35 Sv,

✉ Oleg A. Saenko  
oleg.saenko@canada.ca

<sup>1</sup> Canadian Centre for Climate Modelling and Analysis,  
Victoria, BC, Canada

<sup>2</sup> Department of Earth and Atmospheric Sciences, University  
of Alberta, Edmonton, AB, Canada

the dynamic SSH in the northern North Atlantic increased locally by an order of 1 m.

In climate projections for the twenty first century, changes of the SSH typically have complex geographical patterns (e.g., Suzuki et al. 2005; Landerer et al. 2007; Yin et al. 2010; Bouttes et al. 2014; Gregory et al. 2016), with the standard deviation being particularly large in the North Atlantic (Gregory et al. 2016). This, along with interannual climate variability, can attenuate the link between changes in the AMOC rate and SSH field in such simulations (e.g., Landerer et al. 2007). In addition, the AMOC, which can be affected by the warming and freshwater hosing signals, can in turn influence the corresponding SSH patterns. Thus, in general isolating the response of SSH to warming or hosing from its response to changes in the AMOC may not be possible. Instead, we try to separate the warming and hosing patterns in the SSH anomalies. One way of doing this is to force an ocean model with surface fields that represent, for example, the projected changes to surface temperature and meltwater flux, separately and in combination. Such an approach is adopted here. Specifically, we aim to further elaborate on the meltwater-induced changes in the North Atlantic SSH and circulation, complementing the study of L05 in several ways. First, we explore the ocean response to freshwater hosing under two sets of atmospheric forcing fields, corresponding to a present-day-like climate and to a projected warmer climate with a familiar warming amplification north of about 50°N. Second, the forcing in our freshwater hosing experiments is meant to represent meltwater fluxes from the Greenland Ice Sheet (GrIS), with the rates covering recent projections (Little et al. 2016). Finally, we employ a high-resolution (eddy-permitting) ocean model that reproduces not only the large-scale structure of SSH field, but also the observed magnitude of SSH gradients, as detailed in the next section. The importance of using high-resolution models for addressing the impact of freshwater perturbations on the deep ocean ventilation has been noted before (e.g., Myers 2005; Weijer et al. 2012; Den Toom et al. 2014).

Changes in the SSH and deep water formation can be closely connected to changes in the North Atlantic subpolar gyre circulation. Here we consider the response of the depth-integrated boundary transport off the coast of Labrador, which closes the subpolar gyre in the west; i.e., not far from the region of deep convective mixing in the Labrador Sea. The latter process is known to be sensitive to changes in surface buoyancy (e.g., Yashayaev and Loder 2009), so that the corresponding lateral density gradients and transports may also be affected. In addition, we consider the transport off the east coast of Greenland, which is associated with the East Greenland Current that connects the Arctic Ocean to the North Atlantic. The boundary transports are separated into several components, of which the bottom

velocity transport and thermohaline transport are shown to contribute most to the net. The response of the boundary transport components to the imposed GrIS meltwater fluxes and global warming forcing is then analyzed and compared to each other.

## 2 The model and experimental approach

We employ an eddy-permitting configuration of the Nucleus for European Modelling of the Ocean model (NEMO, version 3.4; Madec and the NEMO team 2012) which uses a free-surface formulation and is coupled to a sea-ice model. The NEMO model is configured on the global ORCA025 grid with 46 z-coordinate vertical levels. The horizontal resolution varies with the cosine of latitude, starting with 1/4° at the equator. The model is forced with daily, annually repeating atmospheric fields, consisting of near-surface winds, air temperature and humidity, as well as surface shortwave and longwave radiative fluxes, precipitation and runoff. Hence, interannual variability, which could attenuate the possible link between the AMOC rate and dynamic SSH (e.g., Landerer et al. 2007), is not present in the surface forcing. All forcing fields are derived from climate simulations that are based on the Canadian Earth System Model (CanESM2) (for details on CanESM2, see Yang and Saenko 2012 and references therein). The computation of surface turbulent fluxes and momentum flux is done using one of the bulk formulations incorporated in NEMO (Madec and the NEMO team 2012). The Control experiment (which is also Control+0.0; more details on the model sensitivity experiments are given below) was forced with the atmospheric fields corresponding to a CanESM2 historical run, averaged from 1979 to 2005. Control was run for 150 years starting from a climatological distribution of ocean temperature and salinity. No restoring to observations was employed to try and correct for the model biases, some of which are discussed next. A strongly constrained ocean model would tend to suppress the response to perturbations in surface forcing.

The model reproduces many observed characteristics of the ocean. In particular, the strength of AMOC in Control, defined as the maximum of the mean overturning streamfunction between 20°N–30°N and below 500 m depth, is 16.8 Sv. For comparison, the mean AMOC transport estimated using the RAPID-MOC data from 2004 to 2014 (see Acknowledgements) is about 17.0 Sv. The simulated pattern of the near-surface geostrophic circulation in the North Atlantic, as given by SSH gradients, is compared to an observational estimate in Fig. 1a, c. Overall, there is a good agreement between the two patterns. Locally, there are biases, some of which are related to our use of the simulated, rather than observed, atmospheric fields to force the

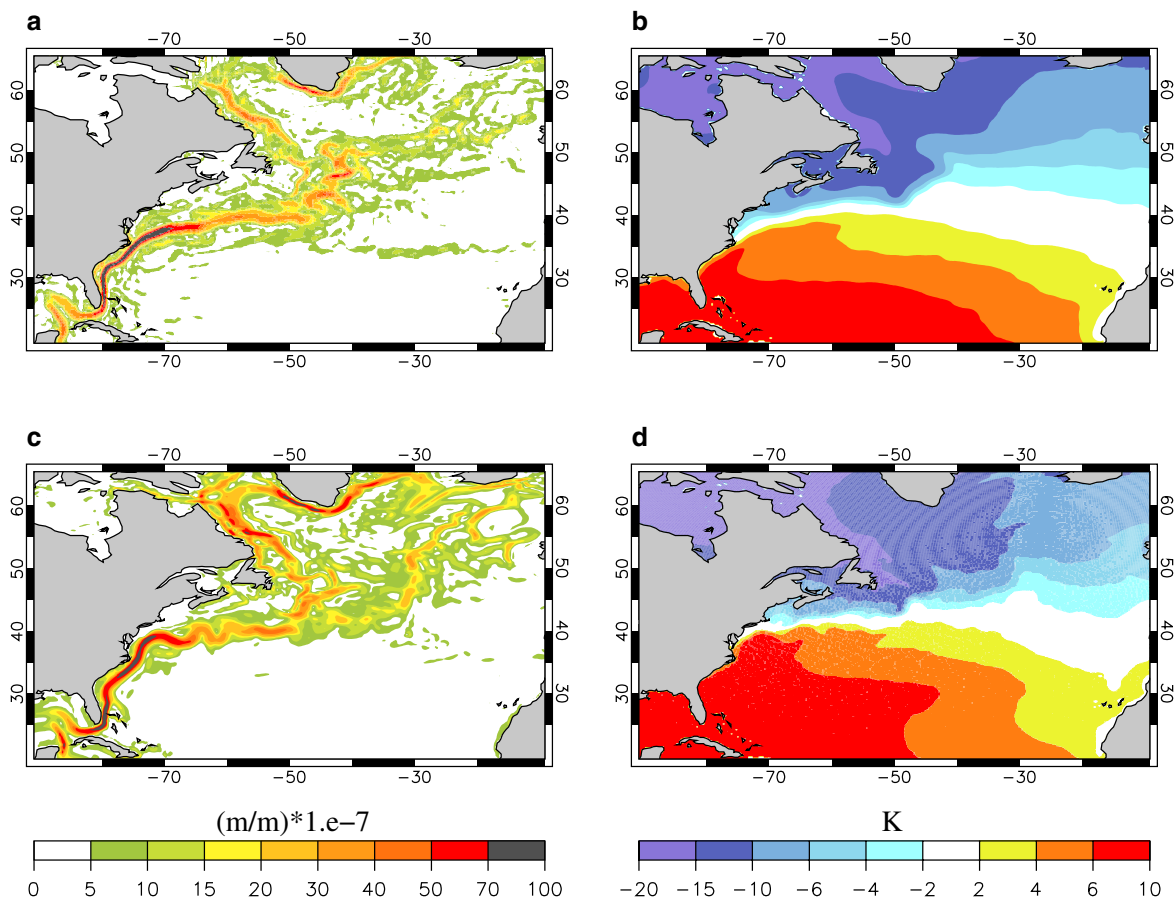


**Fig. 1** **a, c** Magnitude of mean sea surface height (SSH) gradient ( $\text{m m}^{-1}$ ,  $10^{-7}$ ) and **b, d** sea surface temperature (SST) anomaly relative to the global-mean SST: **a, b** observational estimates and **c, d** simulated by the Control experiment (10-year mean fields, representing model years of 141–150). The observational estimate of SSH gradient is based on 10-year mean (2003–2012) SSH AVISO data, whereas the observed climatological mean SST is from the World

Ocean Atlas 2013 version 2 (WOA13 V2) data (Locarnini et al. 2013; see also Acknowledgements). The observational estimates of SSH and SST employed here are on a  $0.25^\circ \times 0.25^\circ$  grid (note that satellite altimetry, by itself, does not measure time-mean flows; the variable used here is *sea surface height above geoid* in AVISO nomenclature)

model. In particular, part of the North Atlantic Current is simulated too far to the east, which is also reflected in the structure of the sea surface temperature (SST) (Fig. 1b, d). In addition, the Gulf Stream (GS) separation from the coast is simulated too far to the north, with the model underestimating the SSH gradients in the GS region. It should also be noted that the atmospheric forcing fields have biases that are likely further amplified by a rather low horizontal resolution,  $\sim 1^\circ$ , in the CanESM2 ocean (Yang and Saenko 2012). However, we found that NEMO, with the employed horizontal resolution of  $1/4^\circ$ , captures many aspects of the observed ocean much better than does the CanESM2's ocean under the same atmospheric forcing, particularly in the subpolar North Atlantic (Saenko et al. 2015). More details on the model parameters and physical parameterizations, as well as on its ability to reproduce some other observations (e.g., eddy kinetic energy, surface heat flux) can be found in Saenko et al. (2015).

We analyze two sets of model sensitivity experiments, Control+N and Warm+N, where the index N takes values of 0.0, 0.025, 0.05, 0.075 and 0.1 and indicates the imposed GrIS meltwater flux in Sv (hereafter “meltwater” effect). For example, in Control+0.05 and Warm+0.05 a freshwater flux of 0.05 Sv was added uniformly along the southern coast of Greenland (Fig. 2a). Thus, the nature of the applied meltwater forcing is highly idealized. It should be noted that the spatial distribution and the rate of future freshwater fluxes from the GrIS are both highly uncertain. Some climate models, with dynamic ice sheet submodels, do predict that most of the GrIS melting will occur along the southern margin of Greenland (Gierz et al. 2015). As for the rate, Little et al. (2016) estimate that by the end of the twenty first century, and for a high-end emission scenario, the GrIS freshwater flux anomaly may reach  $800\text{--}1700 \text{ km}^3 \text{ year}^{-1}$  ( $\sim 0.025\text{--}0.05$  Sv). Thus, the largest GrIS meltwater rate imposed in our model experiments

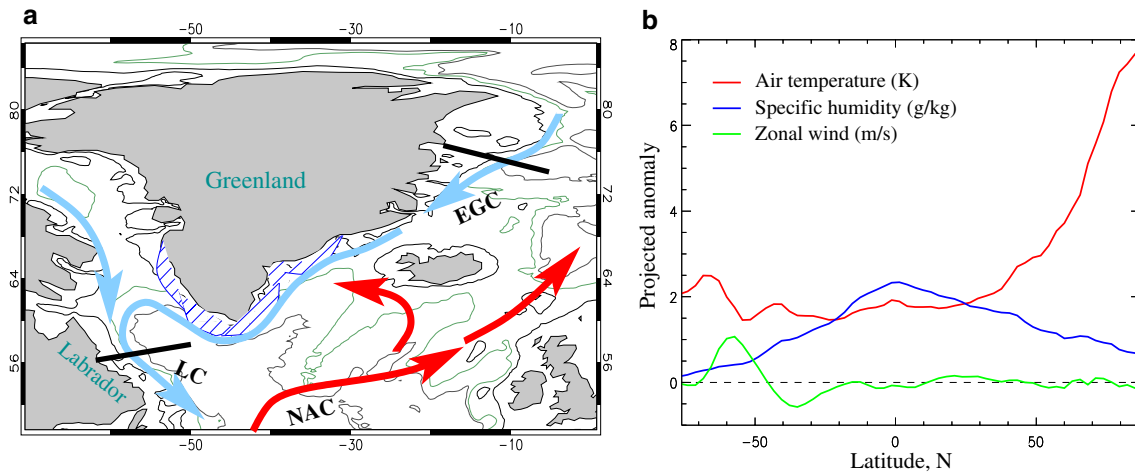


**Fig. 2** **a** A schematic view of the northern North Atlantic Ocean circulation. The *blue* and *red* arrows illustrate the major cold and warm current systems, with “LC”, “EGC” and “NAC” standing for the Labrador Current, East Greenland Current and North Atlantic Current. The hatched region around the southern part of Greenland shows approximately where the meltwater fluxes are introduced to the ocean in the model freshwater hosing experiments. Also shown are the two sections, off the coast of Labrador and off the east coast of Greenland,

that are discussed in the text with regard of the LC and EGC transports. The contours correspond to (*dark*) the 300 and 3000-m isobaths and (*green*) 2000-m isobath, as resolved by the model bathymetry. **b** Zonally averaged (over the ocean) changes in the near-surface air temperature (*red* K), specific humidity (*blue*  $\text{g kg}^{-1}$ ) and zonal wind (*green*  $\text{m s}^{-1}$ ) projected by CanESM2 by the end of the twenty first century (2091–2100) under RCP4.5 scenario

(0.1 Sv) is two times higher than its upper limit estimated for the twenty first century (but is still four times lower than the largest freshwater flux considered by L05). The use of higher meltwater rates is justified, given a steady increase in the projected GrIS freshwater fluxes (Little et al. 2016).

In Control+N, the atmospheric forcing is the same as in Control, whereas in Warm+N it corresponds to the mean climate conditions projected by CanESM2 under the Representative Concentration Pathways scenario 4.5 (RCP4.5; see Moss et al. 2010) by the end of the twenty first century (years 2091–2100). Figure 2b shows the meridional structure of the projected anomalies of surface air temperature (SAT), specific humidity and zonal wind (over the ocean). Under the RCP4.5 scenario, CanESM2 projects an increase in the global-mean SAT of about 2.4 K, with a familiar warming amplification north of 50°N; the projected wind anomalies are largest in the Southern Ocean. The associated changes in the surface fluxes of heat, water and momentum are all represented in the Warm+N set of experiments. We shall refer to their combined influence on the quantities of interest here as to the “warming” effect. The Warm+0.0 experiment was also discussed in Saenko et al. (2015), where it was run for 30 years and called the Full Forcing experiment.

Thus, a total of ten experiments are analyzed here. The model sensitivity experiments were branched off from the Control experiment at year 100 and run for 50 years. Unless stated otherwise, the presented analysis is focused on the fields averaged over the last 10 years in each experiment.

It should be noted that the response to the hosing, which continues to add freshwater to the ocean during the integration, is transient. However, it was found that 50 years was enough for the quantities of our main interest to largely adjust to the imposed forcing perturbations, consistent with Weijer et al. (2012). In addition, our simulations are long enough to make useful comparisons of our results with some other related studies with the same (or similar) duration of imposed GrIS melting rate, ranging from 0.0275 Sv in Stammer et al. (2011) to 0.1 Sv in Weijer et al. (2012) and Swingedouw et al. (2013).

### 3 Results

#### 3.1 Dynamic sea level and AMOC

In this section, we consider the changes in the North Atlantic SSH and AMOC and in some related quantities. In both sets of model experiments, Control+N and Warm+N, the meltwater fluxes result in a weaker AMOC (Fig. 3a), as expected. In particular, the AMOC strength decreases by about 3.0 Sv from Control+0.0 to Control+0.1 (18%) and by 3.6 Sv from Warm+0.0 to Warm+0.1 (24%). The warming effect (Warm+0.0 relative to Control+0.0) decreases the AMOC rate by 1.9 Sv (11%). For comparison, projections of the AMOC weakening by the end of the twenty first century under the RCP4.5 scenario range from 5 to 40% (Cheng et al. 2013).

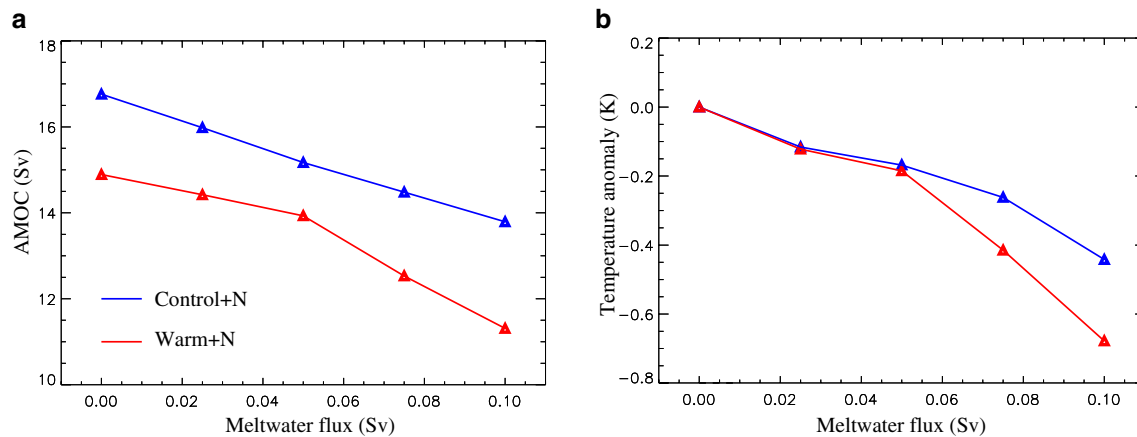


**Fig. 3** **a** The maximum AMOC rate (Sv) in Control+N and Warm+N and **b** changes in the upper 100-m ocean temperature, averaged between 50°N–80°N and 0°–60°W in the North Atlantic, in Control+N and Warm+N relative to, respectively, Control+0.0 and

Warm+0.0. The quantities are plotted as functions of the imposed GrIS meltwater flux; in the adopted notations (i.e., Control+N and Warm+N) index *N* indicates the GrIS meltwater flux in Sv

In general, the net AMOC changes (i.e., changes in Warm+N relative to Control+0.0) cannot be obtained by adding the changes due to the warming (Warm+0.0 relative to Control+0.0) and meltwater (Control+N relative to Control+0.0) effects simulated separately. For example, for the GrIS meltwater flux of 0.1 Sv, the combined (warming + meltwater) effect gives a drop in the AMOC rate of 4.9 Sv, which is smaller than the corresponding net AMOC decrease of 5.4 Sv in Warm+0.1 relative to Control+0.0. In contrast, for the GrIS meltwater flux of 0.05 Sv the AMOC rate drops by 3.5 Sv when the warming and meltwater effects are added, which is larger than the corresponding net AMOC decrease of 2.8 Sv in Warm+0.05 relative to Control+0.0.

With the weakening of the AMOC in response to the GrIS meltwater forcing the upper ocean temperature in the northern North Atlantic (between 50°N and 80°N) decreases (Fig. 3b). For the meltwater fluxes larger than 0.05 Sv this temperature decrease depends on the surface climate, being stronger in Warm+N than in Control+N. For comparison, for the adopted climate change scenario the warming forcing leads to an increase of the upper ocean temperature in the same region by 1.77 °C in Warm+0.0 relative to Control+0.0; i.e., the net warming of the upper northern North Atlantic ocean is still considerably larger than the cooling associated with the hosing.

A weakening of the AMOC is often related to a decrease in the mixed layer depth (MLD) in the northern North Atlantic. This quantity is presented in Fig. 4. In response to the freshwater forcing, the depth of convective mixing decreases in the Labrador Sea and Nordic Seas in both Control+N (Fig. 4, left panels) and Warm+N (Fig. 4, right panels). This is broadly consistent with the impact of 0.1 Sv of Greenland meltwater on the MLD in the models

analyzed by Swingedouw et al. (2013). In response to the warming forcing, the MLD decreases in the Labrador Sea but increases in the Nordic Seas (in all Warm+N runs relative to the corresponding Control+N runs). (Long-term and opposite changes of convective activity in the the Greenland Sea and Labrador Sea were also reported by Dickson et al. (1996), who related them to the phases of the North Atlantic Oscillation). In our model experiments, the increase in the deep convective mixing in the Nordic Seas is related to a retreat of sea-ice in response to the warming (Fig. 4) and enhanced heat loss in the region (Fig. 5a, b; see also Saenko et al. 2015). In addition, the warming causes large positive heat flux anomalies in the Labrador Sea, consistent with the CMIP5 model-mean heat flux change (Bouttes et al. 2014; Gregory et al. 2016), and negative heat flux anomalies in the GS separation region (Fig. 5a, b). The meltwater forcing, through its impact on the AMOC and heat transport, results in mostly positive heat flux anomalies in the northern North Atlantic (typically implying less heat loss by the ocean), with magnitudes which depend on the surface climate conditions. In particular, in the Nordic Seas the heat flux anomaly is stronger in Control+0.05 relative to Control+0.0 than in Warm+0.05 relative to Warm+0.0 (Fig. 5c, d). This is presumably related to the expansion of sea-ice cover in the region in Control+N (Fig. 4, left panels), which tends to decrease heat loss by the ocean. In contrast, in Warm+N the Nordic Seas are mostly ice-free even in winter (Fig. 4, right panels), which favours stronger heat loss.

The combined effect of warming and hosing on the heat flux anomalies are presented in Fig. 5e, f for the meltwater flux of 0.05 Sv. The corresponding net heat flux change (i.e., Warm+0.05 relative to Control+0.0; not shown) can be obtained by either taking the mean between the patterns



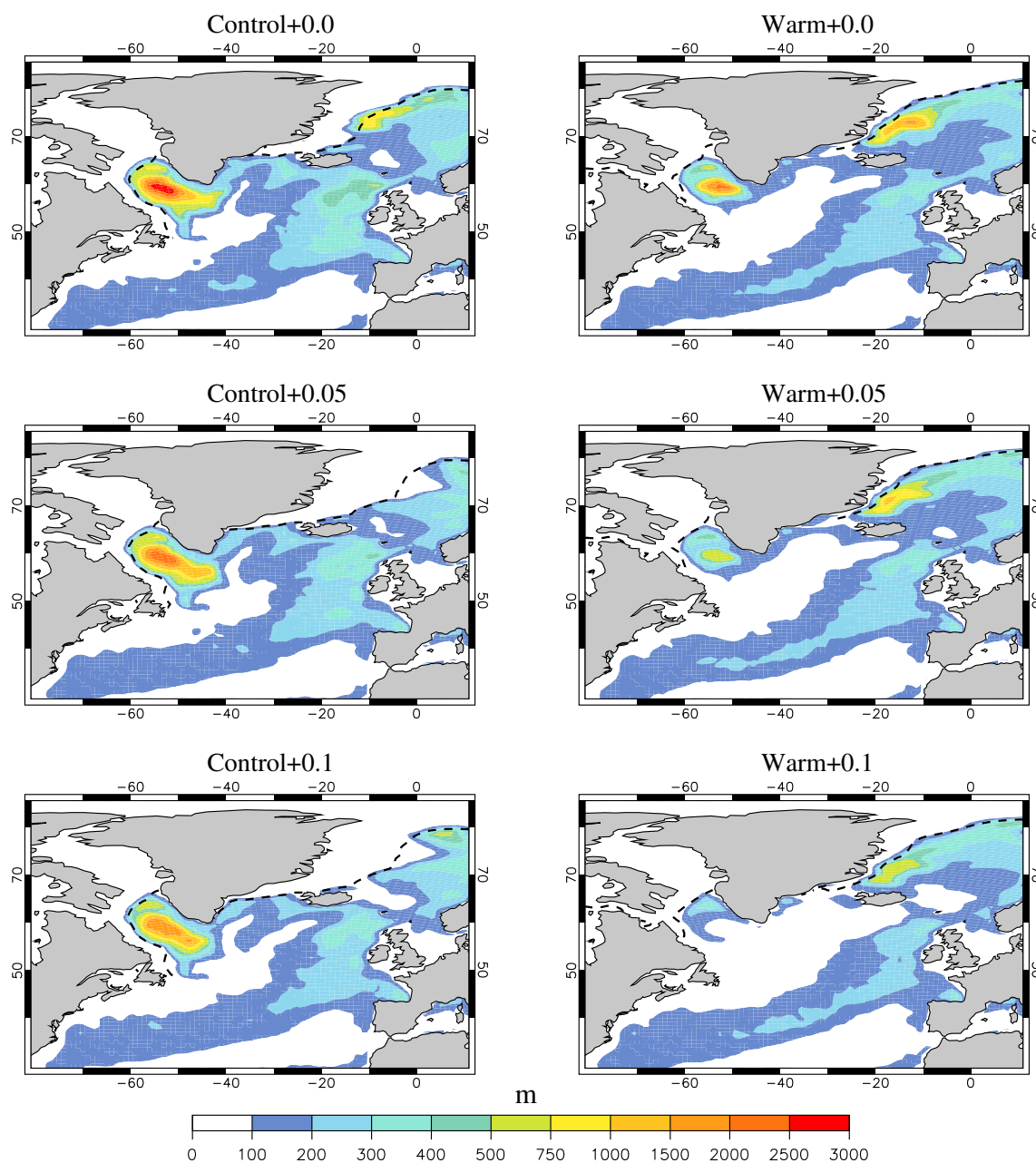


**Fig. 4** Mixed layer depth (color m) and sea-ice cover (dashed contour ice concentration = 0.2) in the North Atlantic in winter (January–March), corresponding to (left) Control+N and (right) Warm+N,

with N taking values of 0.0, 0.05 and 0.1 and indicating the rate of meltwater input (in Sv)

in Fig. 5e, f or by adding the patterns in Fig. 5a, d (or in Fig. 5b, c). For the adopted climate change scenario and GrIS meltwater fluxes of up to 0.05 Sv (which roughly corresponds to the upper limit projected by Little et al. 2016), the net change in the surface heat flux is dominated by the warming effect.

Figure 6 presents the geographical distribution of the dynamic SSH changes in the North Atlantic corresponding to the warming and meltwater effects, separately and in

combination. The patterns have complex structures and, in some places, resemble the corresponding heat flux anomalies in Fig. 5. In particular, the impact of warming on the SSH, which depends on the hosing (Fig. 6a, b), leads to positive SSH anomalies north of the GS and in the Labrador Sea (indicating a weakening of the North Atlantic subpolar gyre discussed in the next section) and to negative SSH anomalies in the subtropical North Atlantic, Irminger Sea and Nordic Seas (relative to the global-mean). This is

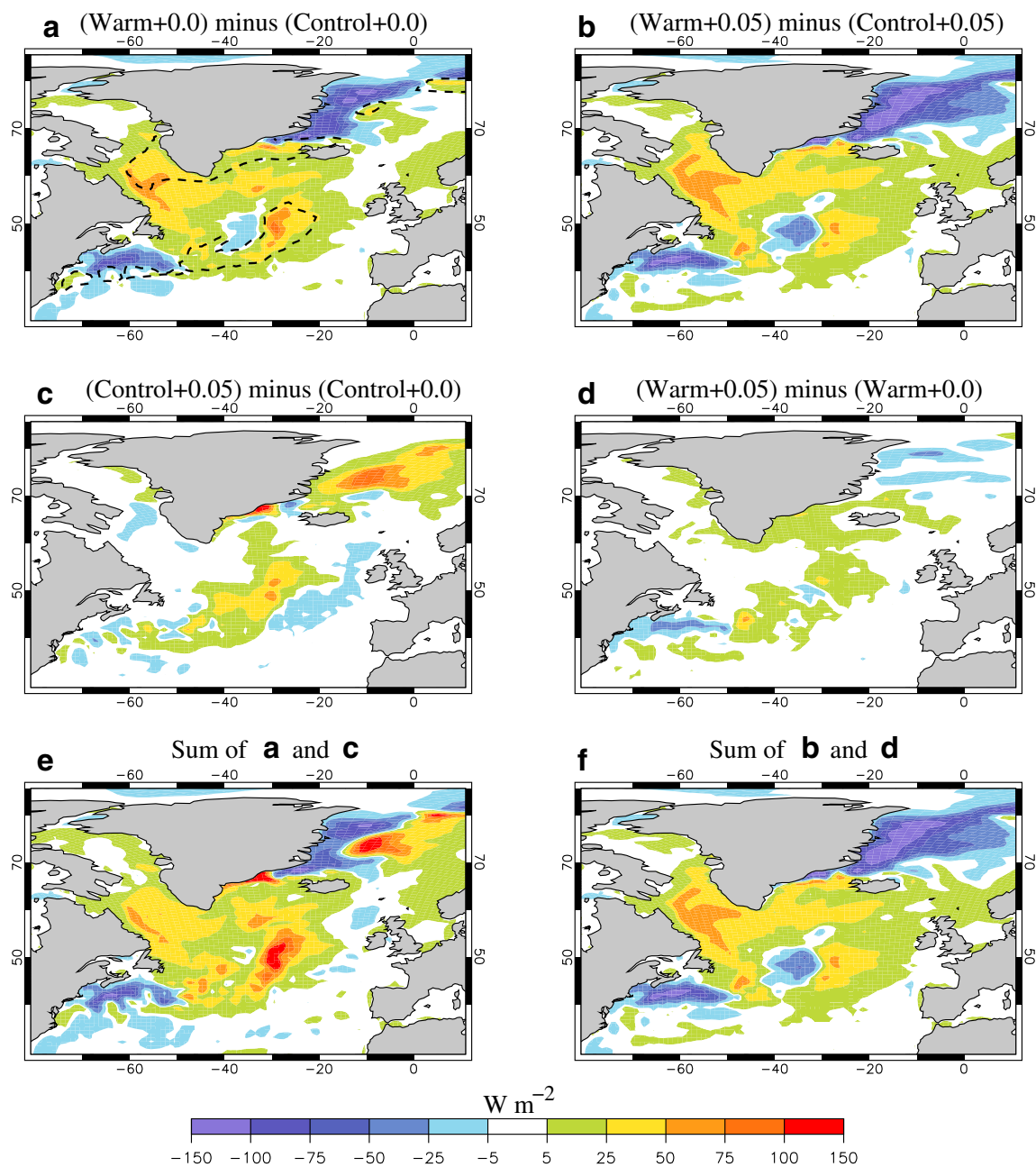


**Fig. 5** Changes in the time-mean surface heat flux ( $\text{W m}^{-2}$ ) in the North Atlantic in **a** Warm+0.0 relative to Control+0.0, **b** Warm+0.05 relative to Control+0.05, **c** Control+0.05 relative to Control+0.0, **d** Warm+0.05 relative to Warm+0.0, **e** the sum of changes in **a**, **c** and **f** the sum of changes in **b**, **d**. Negative values indicated heat loss by

the ocean. In the adopted notations (i.e., Control+N and Warm+N) index  $N$  indicates the meltwater flux (in Sv) applied along the coast of Greenland (see Fig. 2a and text for details). Shown in **a** with dashed contour are the regions where mean heat loss by the ocean exceeds 100  $\text{W m}^{-2}$  in Control+0.0

in general agreement with sea level projections based on climate change scenarios (e.g., Suzuki et al. 2005; Landerer et al. 2007; Yin et al. 2010), including with the CMIP5 model-mean SSH change (Bouttes et al. 2014; Gregory et al. 2016). The drop of the mean SSH in the Nordic Seas, simulated under the warmer climate conditions (Fig. 6a, b), generally implies a stronger cyclonic circulation (cf.

Lique et al. 2014). In our model this is caused, at least in part, by stronger heat loss in the region (Fig. 5a, b) and deeper convective mixing, favoured by sea-ice retreat in the Warm+N runs relative to the corresponding Control+N runs (Fig. 4). As a result, the area-averaged SSH in the Nordic Seas region is roughly the same in Warm+0.1 and Control+0.0, relative to their global-mean values, while the

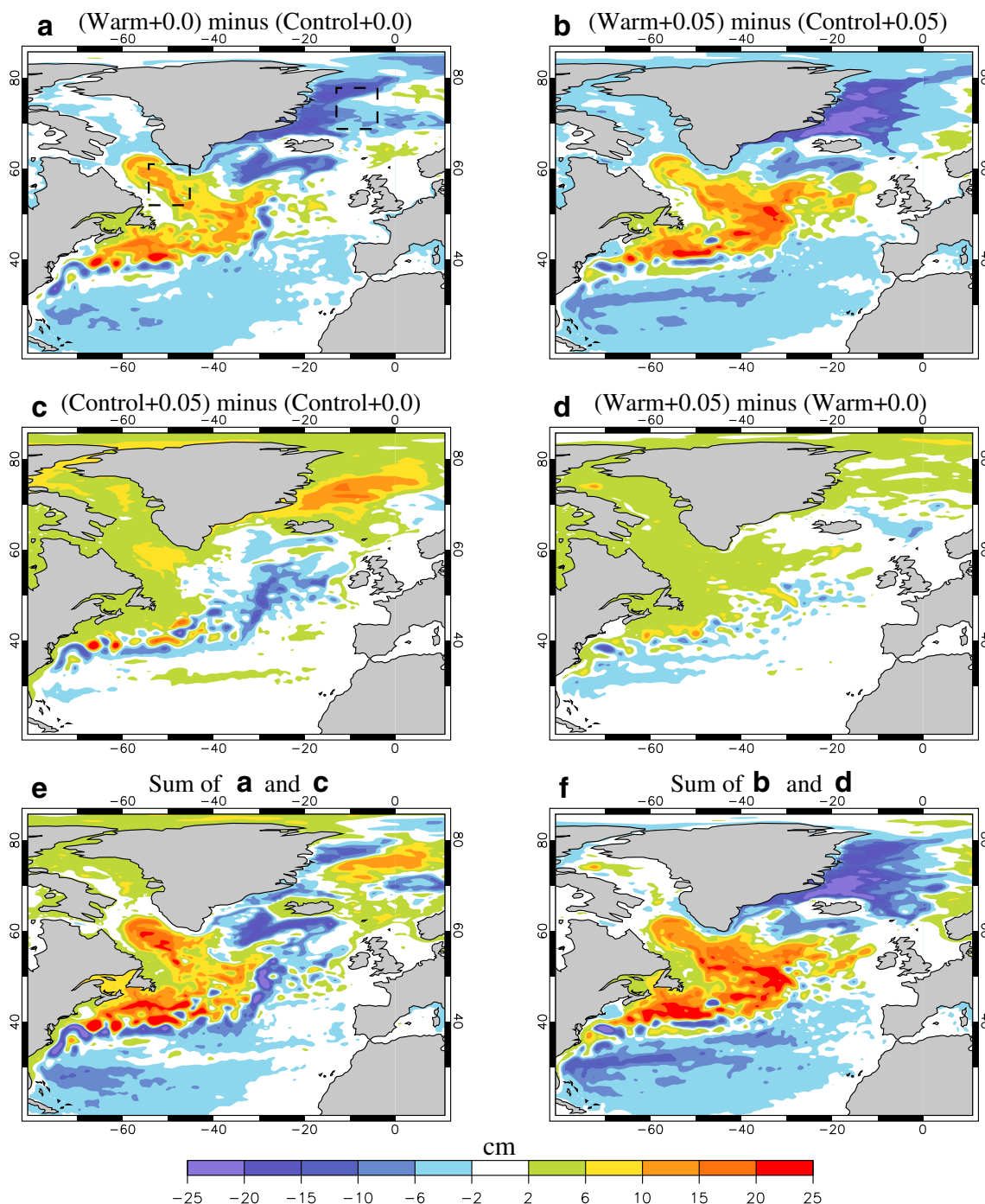


**Fig. 6** Changes in the North Atlantic dynamic SSH (cm) in **a** Warm+0.0 relative to Control+0.0, **b** Warm+0.05 relative to Control+0.05, **c** Control+0.05 relative to Control+0.0, **d** Warm+0.05 relative to Warm+0.0, **e** the sum of changes in **a**, **c** and **f** the sum of changes in **b**, **d**. The global mean values are subtracted. In the

adopted notations (i.e., Control+N and Warm+N) index *N* indicates the meltwater flux (in Sv) applied along the coast of Greenland (see Fig. 2a and text for details). The *two boxes* in **a** indicate the Labrador Sea and Nordic Seas regions discussed in the text

corresponding AMOC rates are, respectively, 11.3 and 16.8 Sv (Fig. 7b). This suggests that the link between the SSH in the northern North Atlantic and AMOC can be more complex than proposed in L05.

The impact of hosing on the SSH, which depends on the warming (Fig. 6c, d), leads to mostly positive SSH changes in the Labrador Sea (see also Fig. 7a). This is consistent with the weakening of deep convective mixing in the



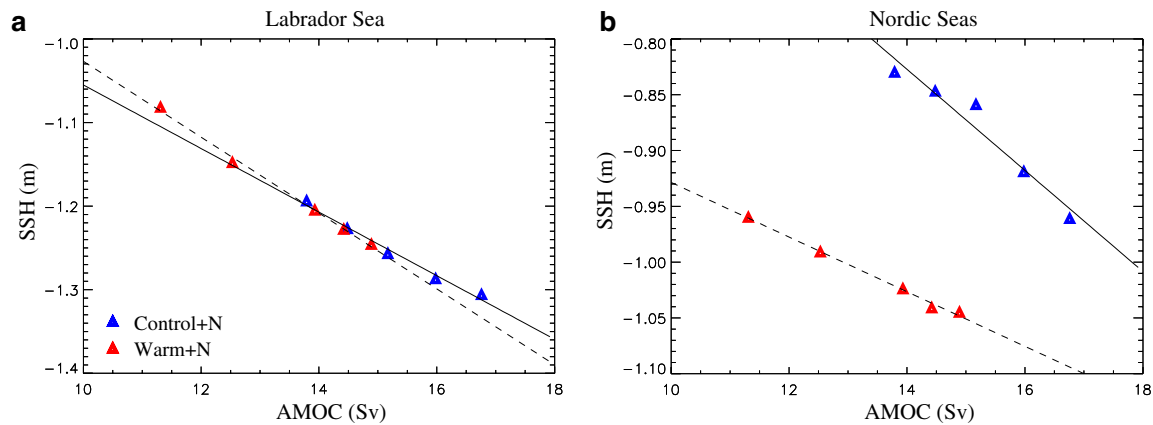


**Fig. 7** Mean dynamic SSH in **a** the Labrador Sea box and **b** the Nordic Seas box plotted against the AMOC rate averaged between 20°N and 30°N. The location of the boxes is shown in Fig. 6a. The lines are regressions for (solid) the Control+N and (dashed) Warm+N sets of experiments (with N taking values of 0.0, 0.025, 0.05, 0.075 and 0.1

and indicating the rate of meltwater input (in Sv) applied along the coast of Greenland; see text for details). The global mean values are subtracted. Note that in both sets of experiments, the higher AMOC rates correspond to the smaller meltwater flux (see Fig. 3a)

Labrador Sea in response to the hosing (Fig. 4) and is in general agreement with the impact of GrIS meltwater fluxes on the SSH patterns presented by Stammer et al. (2011) and Swingedouw et al. (2013); particularly in their model with 1/2° ocean resolution). In the Nordic Seas, the basin-scale SSH also increases with the hosing, which generally implies a reduction of cyclonic circulation in the region (see also next section). However, the increase is larger in Control+N than in Warm+N (see Fig. 7b). In particular, the large positive SSH anomaly in the Nordic Seas in Control+0.05 relative to Control+0.0 (Fig. 6c) is related to the positive heat flux anomaly in the region (Fig. 5c) and to the associated weakening of deep convective mixing (Fig. 4). Thus, even though the Nordic Seas are not directly affected by the meltwater forcing, the deep mixing and SSH in the region can still be affected through indirect effects (e.g., changes in surface heat flux). In addition, the weaker deep water formation in the Nordic Seas can decrease the supply of high-salinity waters to the region from lower latitudes, further affecting the local convective activity and SSH. However, the positive SSH anomaly in the Nordic Seas is much reduced when the meltwater forcing is applied together with the warming forcing (Fig. 6d). This is related to the sea-ice retreat, stronger heat loss and enhanced deep mixing in the region in response to the warming forcing (Figs. 4, 5a, b).

Similar to the net heat flux anomalies, the combined (warming + meltwater) SSH anomalies are dominated in most places by the warming effect (Fig. 6e, f). This applies at least for the GrIS meltwater fluxes of up to 0.05 Sv (which roughly corresponds to the upper limit projected by Little et al. 2016). The corresponding net SSH change (Warm+0.05 relative to Control+0.0; not shown) can be

obtained by either taking the mean between the SSH anomalies in Fig. 6e, f or by adding the anomalies in Fig. 6a, d (or in Fig. 6b, c). It is interesting to note that the simulated patterns of SSH change, particularly the sea level rise in the North Atlantic subpolar gyre and its drop in the subtropics (Fig. 6e, f), resemble the sea level trends in these regions (relative to the global-mean trend) estimated based satellite altimetry for the period 1993–2010 (Stammer et al. 2013; their Fig. 5a). (Stammer et al. 2013 point out that the observed region sea level changes may not yet be related to anthropogenically forced long-term trends, but may instead represent natural modes of climate variability).

Focusing on the two main regions of deep water formation—the Labrador Sea and Nordic Seas—the corresponding area-averaged SSH increases with the decrease of the AMOC rate both in Control+N and Warm+N (Fig. 7). In the Labrador Sea (Fig. 7a), the rates of SSH change with the AMOC strength are comparable in Control+N and Warm+N. The corresponding regression slopes,  $-3.8 \times 10^{-2} \text{ m Sv}^{-1}$  and  $-4.4 \times 10^{-2} \text{ m Sv}^{-1}$ , are in good agreement with the scaling analysis and numerical experiments presented by L05. In the Nordic Seas (Fig. 7b), the SSH-AMOC regression slopes are  $-4.6 \times 10^{-2} \text{ m Sv}^{-1}$  for Control+N and  $-2.4 \times 10^{-2} \text{ m Sv}^{-1}$  for Warm+N. This difference in the slope arises mostly due to the faster increase of the local SSH in Control+N relative to Control+0.0, compared to Warm+N relative to Warm+0.0, for the GrIS meltwater flux of 0.05 Sv and lower (see also Figs. 6c, d, 8b).

To better understand the relative influence of the thermal and haline factors on the SSH response to the imposed meltwater fluxes, it is helpful to consider the sea level changes due to the steric effect,  $\Delta\zeta_s = -(1/\rho_0) \int_{-H}^0 \Delta\rho \, dz$ , partitioning it

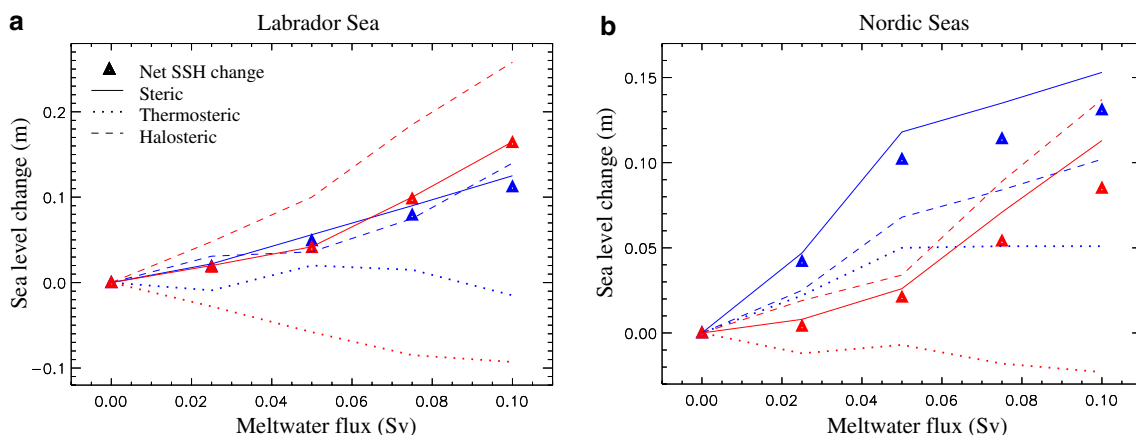


**Fig. 8** Changes in the net dynamic SSH and in sea level due to steric, thermosteric and halosteric effects in (blue) Control+N and (red) Warm+N relative to, respectively, Control+0.0 and Warm+0.0. The sea level changes are plotted as functions of the imposed GrIS melt-

water flux (Sv) for **a** the Labrador Sea box and **b** the Nordic Seas box. The location of the boxes is shown in Fig. 6a. The global mean values are subtracted

into the thermosteric ( $\Delta\zeta_s^{thermo}$ ) and halosteric ( $\Delta\zeta_s^{halo}$ ) contributions, as follows (e.g., Yin et al. 2010):

$$\Delta\zeta_s^{thermo} = -\frac{1}{\rho_0} \int_{-H}^0 [\rho(T, S_r, P_r) - \rho(T_r, S_r, P_r)] dz \quad (1)$$

and

$$\Delta\zeta_s^{halo} = -\frac{1}{\rho_0} \int_{-H}^0 [\rho(T_r, S, P_r) - \rho(T_r, S_r, P_r)] dz, \quad (2)$$

where  $\rho$  is the in situ density,  $T$ ,  $S$ ,  $P$  are, respectively, the temperature, salinity and pressure, with subscript  $r$  indicating their values in a reference state;  $\rho_0$  is a constant density of seawater. Using Control+0.0 and Warm+0.0 as the reference states for, respectively, Control+N and Warm+N, the changes in the steric sea level (relative to the corresponding global mean values) closely follow the changes in the net dynamic SSH anomalies in the Labrador Sea and in the Nordic Seas (Fig. 8). The halosteric effects lead to an increase of the basin-scale  $\Delta\zeta_s$  in both regions, indicating a net freshening. In the Labrador Sea, the freshening is stronger in Warm+N than in Control+N (see also Fig. 9c, d). Averaged over a broader region of the northern North Atlantic, between 50°N–80°N and 0°–60°W, the volume-mean salinity decrease (which is reflected in  $\Delta\zeta_s^{halo}$ ) is about 0.02 g kg<sup>-1</sup> in Control+0.05 (relative to Control+0.0) and 0.04 g kg<sup>-1</sup> in Warm+0.05 (relative to Warm+0.0). This is smaller than the salinity decrease implied by the direct meltwater input of 0.05 Sv over 50 years, which would lead to a drop of the volume-mean salinity in the same region by about 0.2 g kg<sup>-1</sup>. This indicates the important role of ocean dynamics in “mitigating” the impact of

meltwater addition to the northern North Atlantic. Also, in the Labrador Sea (Fig. 8a), while the changes in  $\Delta\zeta_s$  (relative to the global mean values) closely follow each other in Control+N and Warm+N, the corresponding contributions due to  $\Delta\zeta_s^{thermo}$  and  $\Delta\zeta_s^{halo}$  are quite different:  $\Delta\zeta_s^{thermo}$  is negative in Warm+N and does not change much in Control+N, while  $\Delta\zeta_s^{halo}$  is positive and considerably larger in Warm+N than in Control+N. In the Nordic Seas (Fig. 8b) the  $\Delta\zeta_s^{thermo}$  contribution is negative in Warm+N, but positive in Control+N.

Figure 9 displays the patterns of  $\Delta\zeta_s^{thermo}$  and  $\Delta\zeta_s^{halo}$  in the North Atlantic for Control+0.05 (relative to Control+0.0) and for Warm+0.05 (relative to Warm+0.0). North of about 50°N,  $\Delta\zeta_s^{halo}$  is mostly positive both in Control+0.05 and Warm+0.5 (Fig. 9c, d), while  $\Delta\zeta_s^{thermo}$  is mostly negative in Warm+0.05, but has a more complex structure in Control+0.05 (Fig. 9a, b). In particular, in the Nordic Seas,  $\Delta\zeta_s^{thermo}$  is mostly positive in Control+0.05, which is in part due to the positive heat flux anomaly in the region (Fig. 5c), but it is negative in Warm+0.05 (see also Fig. 8b). In the Labrador Sea region,  $\Delta\zeta_s^{thermo}$  is negative in Warm+0.05, indicating a net cooling (relative to Warm+0.0; Fig. 9b), while, for the Control run (in Control+0.05 relative to Control+0.0), it changes sign between the eastern and western parts of the region (Fig. 9a). As a result, the corresponding area-averaged  $\Delta\zeta_s^{thermo}$  in the region is relatively small (Fig. 8a, blue dotted curve).

Thus, enhanced GrIS meltwater fluxes may lead to differences in the response of sea level, AMOC and ocean thermohaline structure when applied under present-day and projected atmospheric forcing. We next consider how the projected warming and meltwater fluxes may affect the transport of some major boundary currents in the northern North

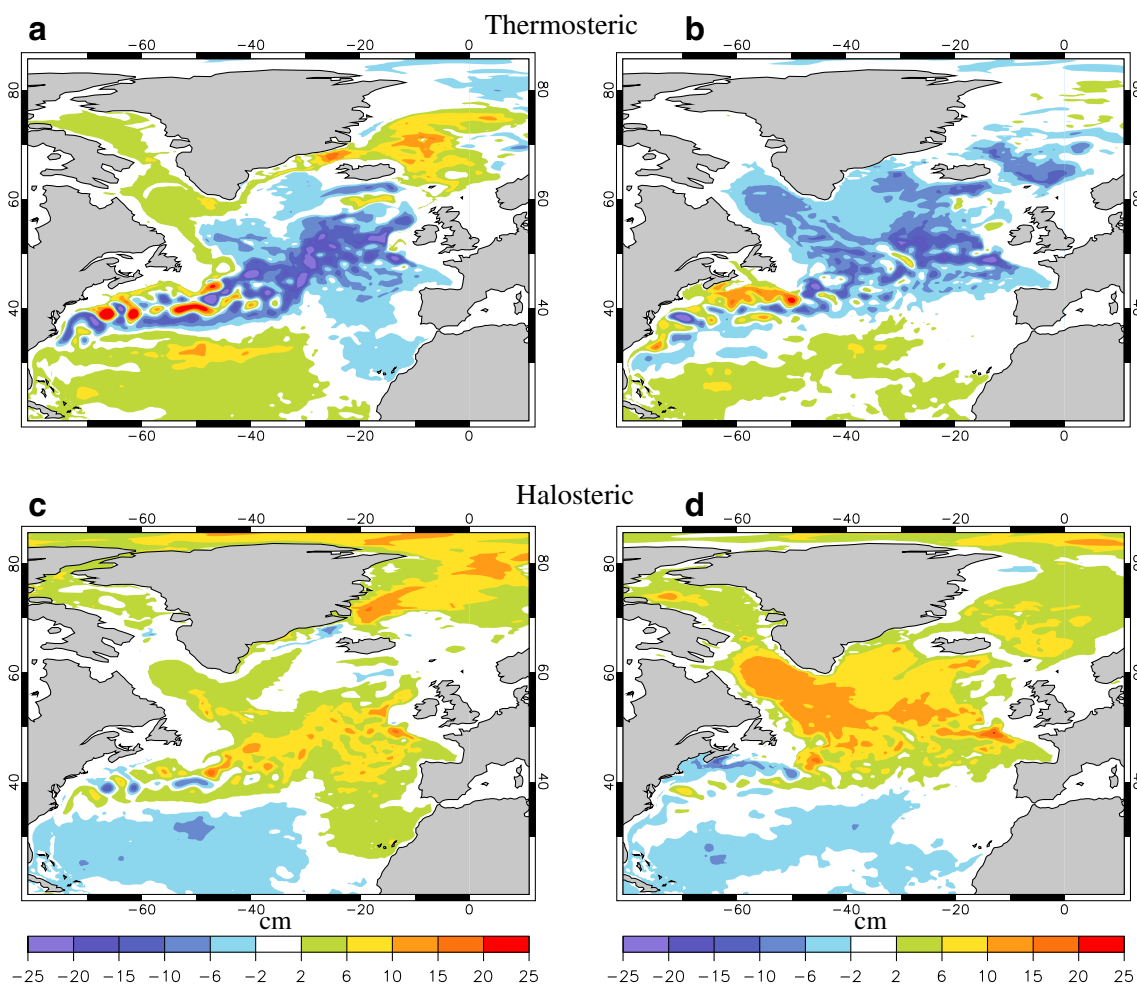


**Fig. 9** Changes in the North Atlantic sea level due to **a, b** thermosteric and **c, d** halosteric effects in **a, c** Control+0.05 relative to Control and in **b, d** Warm+0.05 relative to Warm. The global mean values are subtracted

Atlantic and how the transport changes are related to the changes in the SSH.

### 3.2 Depth-integrated boundary transports

In this section we consider the response to the warming and meltwater forcings of the depth-integrated boundary transports off the coast of Labrador and eastern Greenland (Fig. 2a). The former represents mainly the transport associated with the Labrador Current (LC), which closes the North Atlantic subpolar gyre in the west, whereas the latter is given by the transport of the East Greenland Current (EGC). For the purposes of our analysis it is convenient to write the net depth-integrated velocity across the LC and EGC sections as the sum of the following terms:

$$V \equiv \int_{-H}^0 v \, dz = V_{bt} + V_{th} + V_{ek} + V_{re} \tag{3}$$

where  $V_{bt}$ ,  $V_{th}$  and  $V_{ek}$  represent, respectively, the bottom velocity transport, the thermohaline transport and Ekman transport (e.g., Mellor et al. 1982), whereas  $V_{re}$  is the residual transport (which combines the contributions from the nonlinear terms, horizontal friction, bottom stress and local acceleration). The former three terms are given by (e.g., Mellor et al. 1982; Han and Tang 1999):

$$V_{bt} = \frac{H}{f\rho_0} \frac{\partial P_b}{\partial l} \tag{4}$$

$$V_{th} = \frac{1}{f} \frac{\partial E}{\partial l} \tag{5}$$

$$V_{ek} = -\frac{\tau}{f\rho_0} \tag{6}$$

where  $l$  is the horizontal coordinate along the analyzed section (in our case,  $l = 0$  at the coast to the west of the corresponding section and increases offshore),  $H$

is the bottom topography,  $f$  is the Coriolis parameter;  $P_b = g\rho_0\zeta + g \int_{-H}^0 \rho' dz$  is pressure anomaly at the bottom, with  $g$ ,  $\zeta$  and  $\rho' = \rho - \bar{\rho}$  being, respectively, the gravity, SSH and density anomaly relative to a depth-dependent reference density  $\bar{\rho}(z)$ ;  $E = (g/\rho_0) \int_{-H}^0 z\rho' dz$  is the potential energy;  $\tau$  is the along- $l$  component of surface wind stress. To understand better how changes in the transport are related to changes in the SSH, we shall also decompose  $V_{bt}$  into  $V_{bt}^\zeta$  and  $V_{bt}^\rho$ , which represent the contributions due to the two terms in  $P_b$ , associated with gradients of SSH and density, respectively.

The decomposition (3–6) provides an insight on the relative contribution of baroclinic and barotropic flows to the changes in the boundary transport and corresponding gyre circulation. A similar flow decomposition was applied by Montoya et al. (2011) in their study of the North Atlantic subpolar gyre dynamics in present and glacial climates.

### 3.2.1 The Labrador Current

The transport across a near-zonal section off the coast of Labrador, that roughly follows 57°N (Fig. 2a), is presented in Fig. 10a. It consists of a strong south-eastward (negative) jet-like flow, confined mostly to depths between 300 and 3000 m, a weaker recirculation (positive) and a secondary flow in the interior. The simulated recirculation is not unlike those seen in the Labrador Sea observations and diagnostic calculations (e.g., Lavender et al. 2000; Reynaud et al. 1995). The net southward transports between 300 and 3000-m isobaths is 43.4 Sv, which is in broad agreement with available estimates (e.g., Reynaud et al. 1995). Most of the net transport is

captured by the sum of  $V_{bt}$  and  $V_{th}$ . The relatively small difference between  $V$  and  $V_{bt} + V_{th}$  is more due to  $V_{re}$  than due to  $V_{ek}$ . The contribution of  $V_{bt}$  to the transport between 300 and 3000-m isobaths is larger than  $V_{th}$  (see also Fig. 11b, c). As expected, the  $V_{bt}^\zeta$  component of  $V_{bt}$  dominates the  $V_{bt}^\rho$  component, resulting in the net southward transport due to  $V_{bt}$ . An exception is the region around 3000-m isobath where  $V_{bt}^\rho$  dominates  $V_{bt}^\zeta$ , leading to the recirculations.

The main components of the LC transport for Control+N and Warm+N, integrated between 300 and 3000-m isobaths, are presented in Fig. 11 as functions of the applied GrIS meltwater flux. Both the warming and meltwater forcings lead to a weakening of the depth-integrated transports off the coast of Labrador and to the associated weakening of the North Atlantic subpolar gyre circulation (the rate of which is mostly given by the boundary transport). In particular, the warming effect (change in Warm+0.0 relative to Control+0.0) leads to a decrease in the combined  $V_{bt} + V_{th}$  southward transport by about 7 Sv (Fig. 11a). This is almost exclusively due to  $V_{th}$  (Fig. 11b), whereas  $V_{bt}$  is not affected by the warming at zero meltwater flux (Fig. 11c). The weakening of the  $V_{th}$  contribution to the LC transport is due to the decrease in the depth-integrated  $E$  contrast across the continental slope. This is related to the weaker convective activity and heat loss in the Labrador Sea (Figs. 4, 5a). A similar mechanism, connecting the baroclinic flow, deep mixing in the Labrador Sea interior and surface buoyancy forcing, is discussed by Born and Stocker (2014) using an idealized model. The weak sensitivity of  $V_{bt}$  results from the changes in  $V_{bt}^\zeta$  and  $V_{bt}^\rho$  (Fig. 11d, e) that almost cancel each other at zero meltwater flux (Fig. 11c).

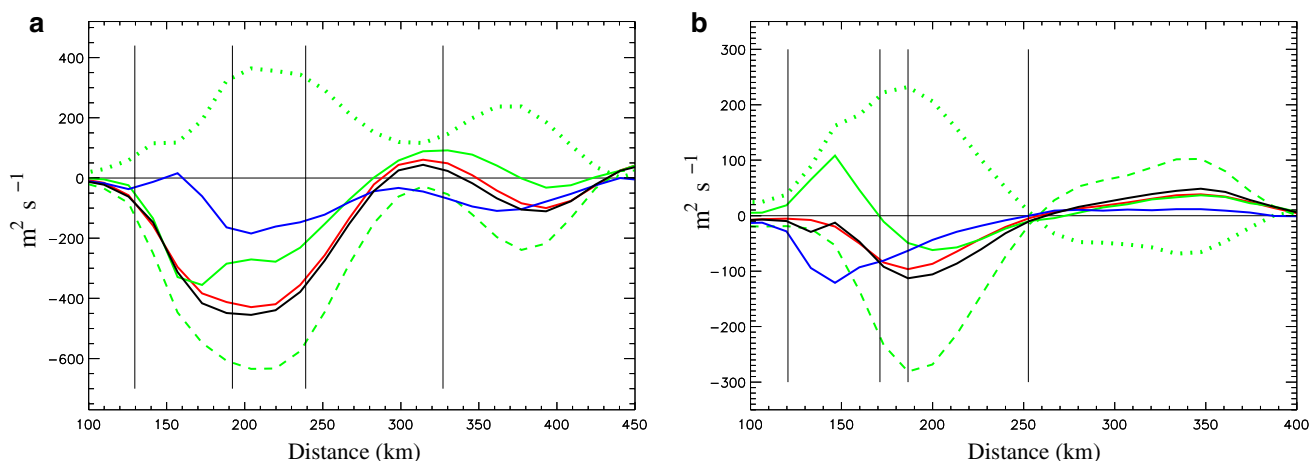


**Fig. 10** Volume transport per unit width ( $m^2 s^{-1}$ ) in Control+0.0 across two sections, around **a** 57°N and **b** 75°N (see Fig. 2a), as function of distance from the coast of **a** Labrador and **b** Greenland: (red) net model transport, (black) the combined bottom velocity and thermohaline transport, (blue) thermohaline transport and (green) bottom

velocity transport. Dashed and dotted curves represent the two components of the bottom velocity transport associated, respectively, with dynamic sea level and density gradients (see text for details). Vertical lines indicate (from left to right) the locations of 300, 2000, 2500 and 3000-m isobaths. Negative values represent southward transports



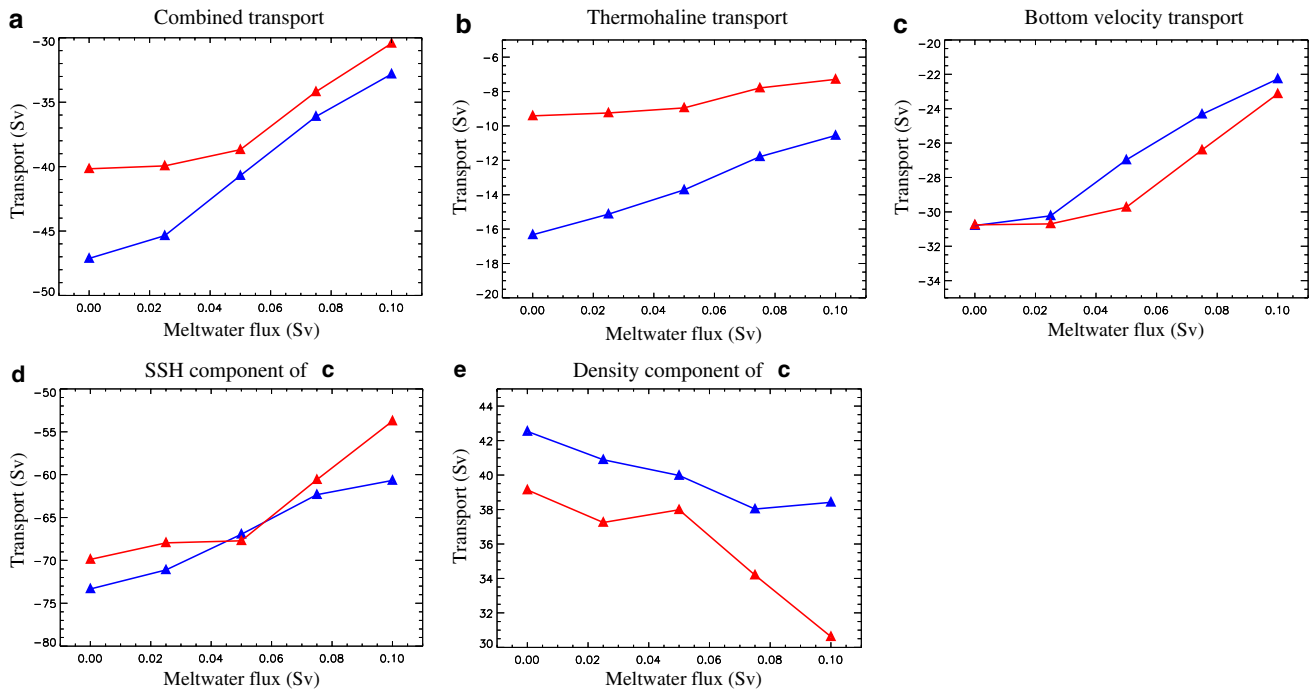


**Fig. 11** Main components of the Labrador Current transport between 300 and 3000-m isobaths, i.e. where most of the southward transport is confined (Fig. 9), as functions of meltwater flux from Greenland: **a** the combined effect of the thermohaline and bottom velocity transports ( $V_{th} + V_{bt}$ ), **b** thermohaline transport ( $V_{th}$ ), **c** bottom velocity transport ( $V_{bt}$ ), **d** contribution of dynamic sea level gradients to  $V_{bt}$  ( $V_{bt}^{\zeta}$ ) and **e** contribution of density gradients to  $V_{bt}$  ( $V_{bt}^{\rho}$ ) (see text for

the definitions). Plotted in *blue* and *red* are, respectively, the transports in the two subsets of model experiments, Control+N and Warm+N, where  $N$  indicates the meltwater flux from Greenland ( $x$ -axis). *Negative values* represent southward transports. The results are shown for the section that roughly follows  $57^{\circ}\text{N}$  (see Fig. 2a); similar results apply to the section at  $59^{\circ}\text{N}$

With the increase of meltwater flux, the impact of the warming on the combined  $V_{bt} + V_{th}$  transport tends to decrease (Fig. 11a). One reason for this is that  $V_{th}$  is not very sensitive to the GrIS meltwater input in Warm+N, whereas its contribution to the LC transport decreases in Control+N (Fig. 11b). The contribution of  $V_{bt}$  also decreases, but both in Control+N and Warm+N (Fig. 11c), particularly when the GrIS meltwater flux exceeds 0.025 Sv. This, in turn, is because the magnitudes of  $V_{bt}^{\zeta}$  decrease faster with the meltwater flux than do the magnitudes of  $V_{bt}^{\rho}$  (Fig. 11d, e).

In Fig. 12 the changes in  $\zeta$  corresponding to  $V_{bt}^{\zeta}$  in Fig. 11d (i.e.,  $\zeta$  at 3000-m isobath minus  $\zeta$  at 300-m isobath across the LC) are plotted against the AMOC rate. The associated regression slopes are  $-2.4 \times 10^{-2} \text{ m Sv}^{-1}$  and  $-2.1 \times 10^{-2} \text{ m Sv}^{-1}$  for Control+N and Warm+N, respectively (cf. Fig. 7a). This implies that, on a long-term mean, a change in the AMOC rate by, for example, 5 Sv would be reflected in a change of the SSH difference across the LC by about 10 cm.

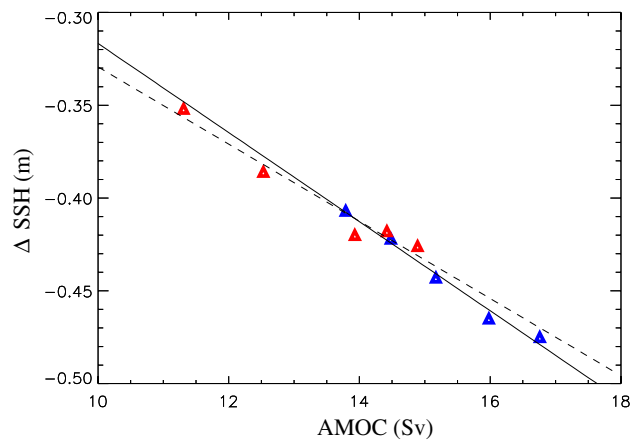


**Fig. 12** The dynamic SSH difference across the Labrador Current (around  $57^{\circ}\text{N}$  and between 3000 and 300-m isobaths) plotted against the AMOC rate averaged between  $20^{\circ}\text{N}$ – $30^{\circ}\text{N}$ . The *lines* are regressions for (*solid*) the Control+N and (*dashed*) Warm+N sets of experiments [with  $N$  taking values of 0.0, 0.025, 0.05, 0.075 and 0.1 Sv and indicating the rate of meltwater input (in Sv) applied along the coast of Greenland; see text for details]. Note that in both sets of experiments, the higher MOC rates correspond to the smaller meltwater flux (see Fig. 3a)

### 3.2.2 East Greenland Current

The transport across a section off the east coast of Greenland, centered roughly on 75°N (Fig. 2a), is presented in Fig. 10b. Its major feature is a south-westward (negative) boundary flow confined to depths between 300 and 3000 m. It represents mainly the EGC—a major component of the Nordic Seas circulation, which also links the Arctic Ocean to the North Atlantic. The combined thermohaline and bottom velocity transport ( $V_{th} + V_{bt}$ ) captures well the net transport of the EGC, similar to the LC, as previously presented. In Control+0.0, it integrates to 7.7 Sv, which is within the uncertainty of the observational estimates presented by de Steur et al. (2014). The main contributor to the net transport is the thermohaline transport ( $V_{th}$ ). The bottom transport ( $V_{bt}$ ), which changes sign along the section, is relatively small when integrated between the 300 and 3000-m isobaths. It is a residual of typically larger transports associated with the SSH and density gradients (Fig. 10b; Table 1).

The combined ( $V_{th} + V_{bt}$ ) EGC transport, its individual components and their response to the warming and meltwater forcings are summarized in Table 1. Compared to the LC transport, the changes in the EGC transport are more complex. In particular, while the combined southward transport decreases with the increase of meltwater forcing, mainly due to the less negative  $V_{th}$ , this only holds for Control+N and for the meltwater fluxes smaller than 0.05 Sv. With the increase of meltwater flux above 0.05 Sv, the EGC transport increases both in Control+N and Warm+N. In Warm+0.075 and Warm+0.1, the changes in  $V_{bt}^{\zeta}$  are not

**Table 1** The combined thermohaline and bottom velocity transport ( $V_{th} + V_{bt}$ ), the thermohaline transport ( $V_{th}$ ) and bottom velocity transport ( $V_{bt}$ ) (in Sv) of the East Greenland Current across the section at ~75°N (see Fig. 2a)

FW flux	$V_{bt} + V_{th}$	$V_{th}$	$V_{bt}$	$V_{bt}^{\zeta}$	$V_{bt}^{\rho}$
0.000	-7.7; -5.9	-7.3; -6.4	-0.4; 0.5	-19.1; -8.1	18.7; 8.6
0.025	-5.8; -6.2	-6.6; -6.2	0.8; 0.0	-17.1; -8.3	17.9; 8.3
0.050	-4.4; -5.5	-5.8; -5.9	1.4; 0.4	-10.7; -6.5	12.1; 6.9
0.075	-4.5; -7.7	-5.4; -5.6	0.9; -2.1	-10.8; -8.9	11.7; 6.8
0.100	-5.2; -8.8	-5.5; -5.8	0.3; -3.0	-14.3; -14.3	14.6; 11.3

The bottom velocity transport is further separated into the contributions from the gradients of dynamic sea level ( $V_{bt}^{\zeta}$ ) and density ( $V_{bt}^{\rho}$ ) ( $V_{bt} = V_{bt}^{\zeta} + V_{bt}^{\rho}$ ; see text for details). The transport values separated by semicolon correspond to (left) Control+N and (right) Warm+N, with N representing the GrIS freshwater (FW) flux (in Sv). Negative values indicate south-westward transports

fully compensated by  $V_{bt}^{\rho}$ , which increases the contribution of  $V_{bt}$  to the southward transport of the EGC. However, the magnitude of  $V_{bt}$  remains smaller than  $V_{th}$ , whereas its two components change considerably in response to the hosing and warming.

The warming forcing increases the EGC transport (except at zero meltwater flux). This is presumably related to the stronger convection in the Nordic Sea, associated with the retreat of sea-ice in response to the warming (Fig. 4). Typically, the response of  $V_{bt}$  to the warming is stronger than the response of  $V_{th}$ . It is interesting to note that the observed recent increase in the EGC transport has been related mostly to an increase in barotropic flow (de Steur et al. 2014).

In general, the changes of the EGC transport, in response to either the GrIS meltwater forcing or the warming or both, are relatively large. They are caused by a complex interplay between the SSH and density anomalies on both sides of the EGC. However, for the considered climate change scenario and GrIS meltwater fluxes the simulated transport changes typically do not exceed the observed interannual variability of the EGC transport (e.g., de Steur et al. 2014).

## 4 Discussion and conclusions

Mean SSH is considerably lower in the northern North Atlantic than in the North Pacific. It is thought that this is in part due to the formation of deep, dense water in the northern North Atlantic and the associated AMOC. However, while connecting the SSH and AMOC changes could be insightful (L05), in general isolating the SSH response to warming or freshwater input from its response to changes in the AMOC may not be possible. Instead, we focus more on separating the warming and hosing patterns in the North Atlantic SSH anomalies. The approach we employ consists of running a set of idealized freshwater hosing experiments with a high-resolution ocean model, forced with atmospheric fields derived from a coupled model. The freshwater forcing in our experiments increases by 0.025 Sv from 0.0 to 0.1 Sv and is meant to represent the enhanced meltwater fluxes from the GrIS in a warmer climate. Hence, the influence of the GrIS meltwater fluxes is explored not only under the present-day-like climate, but also under the climate conditions projected by the end of the twenty first century, with a familiar warming amplification north of about 50°N. It is found that the GrIS meltwater fluxes result in the changes of the North Atlantic SSH that have a complex geographical pattern, while the AMOC rate declines. In particular, in the two major regions of deep water formation—the Labrador Sea and Nordic Seas—the basin-mean SSH increases with the increase of the GrIS meltwater flux. This is related to the reduced convective

activity in both regions in response to the meltwater forcing and holds under the present-day and projected climate conditions, supporting the results of L05. However, while in the Labrador Sea both the warming and meltwater forcing lead to sea level rise, in the Nordic Seas these two effects have an opposite influence on the basin-mean SSH (relative to the corresponding global mean values). This is related to the intensified convective activity in the Nordic Seas in response to the warming, associated with a retreat of sea-ice and enhanced surface heat loss in the region. As a result, the basin-mean SSH in the Nordic Seas is affected less when the meltwater and warming forcings are applied together. In general, the impact of warming on the SSH patterns depends on the hosing and vice-versa.

The imposed perturbations to the surface forcing also have a strong impact on the boundary transports in the northern North Atlantic and the associated gyre circulation. Here, we focus on the depth-integrated boundary transports off the coast of Labrador and eastern Greenland. The former is mainly associated with the LC, whereas the latter—with the EGC. It is found that the LC transport decreases (by about 7 Sv) in response to the projected warming. This decrease is almost exclusively due to the thermohaline transport component. In contrast, the bottom velocity transport is essentially insensitive to the warming, because of the compensating changes in the SSH and density gradients across the LC. With the increase of the GrIS meltwater flux, the LC transport decreases further. This decrease is composed of the contributions from the bottom velocity and thermohaline transports, which both decrease (i.e., become less negative). However, while the bottom velocity transport decreases under both the present-day and projected climate conditions, the thermohaline transport is less sensitive to the GrIS meltwater fluxes under the warmer surface climate. For the two sets of surface climate conditions, the SSH difference across the LC (which is also a component of the bottom velocity transport) correlates well with the (long-term mean) AMOC changes in response to the imposed GrIS meltwater fluxes. This suggests a way for monitoring some impacts of climate change on the large-scale ocean circulation through the use of satellite altimetry. In turn, the simulated changes in the EGC transport are generally more complex than the changes in the LC transport.

**Acknowledgements** We thank reviewers and Cathy Reader for constructive comments. We are grateful to the NEMO development team for providing the model and continuous guidance. We also thank Ed Wiebe for the assistance with the graphics. The gridded, onto a  $1/4^\circ \times 1/4^\circ$  grid, SSH data were obtained from the Archiving, Validation and Interpretation of Satellite Oceanographic data (AVISO) website: <http://www.aviso.altimetry.fr/en/home.html>. The cited RAPID-MOC data is available from <http://www.rapid.ac.uk/rapidmoc>. The World Ocean Atlas 2013 version 2 (WOA13 V2) data is from <https://www.nodc.noaa.gov/cgi-bin/OC5/woa13/woa13.pl>. P.

Myers acknowledges funding from NSERC through the VITALS network (Award 433898-2012).

**Open Access** This article is distributed under the terms of the Creative Commons Attribution 4.0 International License (<http://creativecommons.org/licenses/by/4.0/>), which permits unrestricted use, distribution, and reproduction in any medium, provided you give appropriate credit to the original author(s) and the source, provide a link to the Creative Commons license, and indicate if changes were made.

## References

- Born A, Stocker TF (2014) Two stable equilibria of the Atlantic subpolar gyre. *J Phys Oceanogr* 44:246–264. doi:[10.1175/JPO-D-13-073.1](https://doi.org/10.1175/JPO-D-13-073.1)
- Bouttes N, Gregory JM, Kuhlbrodt T, Smith RS (2014) The drivers of projected North Atlantic sea level change. *Clim Dyn* 43:1531–1544. doi:[10.1007/s00382-013-1973-8](https://doi.org/10.1007/s00382-013-1973-8)
- Cheng W, Chiang JCH, Zhang D (2013) Atlantic meridional overturning circulation (AMOC) in CMIP5 models: RCP and historical simulations. *J Clim* 26:7187–7197
- de Steur L, Hansen E, Mauritzen C, Besczynska-Moller A, Fahrbach E (2014) Impact of recirculation on the East Greenland Current in Fram Strait: results from moored current meter measurements between 1997 and 2009. *Deep Sea Res Part I* 92:26–40. doi:[10.1016/j.dsr.2014.05.018](https://doi.org/10.1016/j.dsr.2014.05.018)
- Den Toom M, Dijkstra HA, Weijer W, Hecht WM, Maltrud ME, van Sebille E (2014) Sensitivity of a strongly eddying global ocean to North Atlantic freshwater perturbations. *J Phys Oceanogr* 44:464–481
- Dickson R, Lazier J, Meincke J, Rhines P, Swift J (1996) Long-term coordinated changes in the convective activity of the North Atlantic. *Prog Oceanogr* 38:241–295
- Gierz P, Lohmann G, Wei W (2015) Response of Atlantic overturning to future warming in a coupled atmosphere–ocean–ice sheet model. *Geophys Res Lett* 42:6811–6818
- Gregory JM, Bouttes N, Griffies SM, Haak H, Hurlin WJ, Jungclauss J, Kelley M, Lee WG, Marshall J, Romanou A, Saenko OA, Stammer D, Winton M (2016) The Flux-Anomaly-Forced Model Intercomparison Project (FAFMIP) contribution to CMIP6: investigation of sea-level and ocean climate change in response to CO<sub>2</sub> forcing. *Geosci Model Dev Discuss* 9:3993–4017. doi:[10.5194/gmd-9-3993-2016](https://doi.org/10.5194/gmd-9-3993-2016)
- Han G, Tang CL (1999) Velocity and transport of the Labrador Current determined from altimetric, hydrographic, and wind data. *J Geophys Res* 104(C8):18047–18057. doi:[10.1029/1999JC900145](https://doi.org/10.1029/1999JC900145)
- Landerer FW, Jungclauss JH, Marotzke J (2007) Regional dynamic and steric sea level change in response to the IPCC-A1B scenario. *J Phys Oceanogr* 37:296–312
- Lavender K, Davis RE, Owens WB (2000) Mid-depth recirculation observed in the interior Labrador and Irminger Seas by direct velocity measurements. *Nature* 407:66–69. doi:[10.1038/35024048](https://doi.org/10.1038/35024048)
- Levermann A, Griesel A, Hofmann M, Montoya M, Rahmstorf S (2005) Dynamic sea level changes following changes in the thermohaline circulation. *Clim Dyn* 24:347–354
- Lique C, Johnson HL, Plancherel Y, Flanders R (2014) Ocean change around Greenland under a warming climate. *Clim Dyn* 45:1235–1252

- Little CM, Piecuch CG, Chaudhuri AH (2016) Quantifying Greenland freshwater flux underestimates in climate models. *Geophys Res Lett* 43:5370–5377. doi:[10.1002/2016GL068878](https://doi.org/10.1002/2016GL068878)
- Locarnini RA, Mishonov AV, Antonov JJ, Boyer TP, Garcia HE, Baranova OK, Zweng MM, Paver CR, Reagan JR, Johnson DR, Hamilton M, Seidov D (2013) World Ocean Atlas 2013, Volume 1: Temperature. In: Levitus S (ed) Mishonov A (Technical ed) NOAA Atlas NESDIS 73, Silver Spring, MD, 40 pp
- Madec G, the NEMO team (2012) NEMO ocean engine. Note du Pole de modelisation, Institut Pierre-Simon Laplace (IPSL), France, No 27 ISSN No 1288-1619
- Mellor GL, Mechoso CR, Keto E (1982) A diagnostic calculation of the general circulation of the Atlantic Ocean. *Deep Sea Res* 29:1171–1192
- Montoya M, Born A, Levermann A (2011) Reversed North Atlantic gyre dynamics in present and glacial climates. *Clim Dyn* 36:1107–1118. doi:[10.1007/s00382-009-0729-y](https://doi.org/10.1007/s00382-009-0729-y)
- Moss RH et al (2010) The next generation of scenarios for climate change research and assessment. *Nature* 463:747–756. doi:[10.1038/nature08823](https://doi.org/10.1038/nature08823)
- Myers PG (2005) Impact of freshwater from the Canadian Arctic Archipelago on Labrador Sea Water formation. *Geophys Res Lett* 32. doi:[10.1029/2004GL022082](https://doi.org/10.1029/2004GL022082)
- Reynaud TH, Weaver AJ, Greatbatch RJ (1995) Summer mean circulation of the northwestern Atlantic Ocean. *J Geophys Res* 100(C1):779–816
- Saenko OA, Yang D, Gregory JM, Spence P, Myers PG (2015) Separating the influence of projected changes in air temperature and wind on patterns of sea level change and ocean heat content. *J Geophys Res Oceans* 120:5749–5765. doi:[10.1002/jgrc.v120.8](https://doi.org/10.1002/jgrc.v120.8)
- Stammer D, Agarwal N, Herrmann P, Kohl A, Mechoso CR (2011) Response of a coupled ocean–atmosphere model to Greenland ice melting. *Surv Geophys* 32:621–642. doi:[10.1007/s10712-011-9142-2](https://doi.org/10.1007/s10712-011-9142-2)
- Stammer D, Cazenave A, Ponte RM, Tamisiea ME (2013) Causes for contemporary regional sea level changes. *Annu Rev Mar Sci* 5:21–46
- Suzuki T, Hasumi H, Sakamoto TT, Nishimura T, Abe-Ouchi A, Segawa T, Okada N, Oka A, Emori S (2005) Projection of future sea level and its variability in a high-resolution climate model: ocean processes and Greenland and Antarctic ice-melt contributions. *Geophys Res Lett* 32:L19706. doi:[10.1029/2005GL023677](https://doi.org/10.1029/2005GL023677)
- Swingedouw D, Rodehacke CB, Behrens E, Menary M, Olsen SM, Gao Y, Mikolajewicz U, Mignot J, Biastoch A (2013) Decadal fingerprints of freshwater discharge around Greenland in a multi-model ensemble. *Clim Dyn* 41:695–720
- Weijer W, Maltrud ME, Hecht MW, Dijkstra HA, Kliphuis MA (2012) Response of the Atlantic Ocean circulation to Greenland Ice Sheet melting in a strongly-eddy ocean model. *Geophys Res Lett* 39:L09606. doi:[10.1029/2012GL051611](https://doi.org/10.1029/2012GL051611)
- Wunsch C (1997) The vertical partition of oceanic horizontal kinetic energy and the spectrum of global variability. *J Phys Oceanogr* 27:1770–1794
- Yang D, Saenko OA (2012) Ocean heat transport and its projected change in CanESM2. *J Clim* 25:8148–8163
- Yashayaev I, Loder JW (2009) Enhanced production of Labrador Sea Water in 2008. *Geophys Res Lett* 36:L01606. doi:[10.1029/2008GL036162](https://doi.org/10.1029/2008GL036162)
- Yin J, Griffies SM, Stouffer RJ (2010) Spatial variability of sea level rise in twenty-first century projections. *J Clim* 23:4585–4607